ACS central science

Research Article

Cite This: ACS Cent. Sci. 2018, 4, 1065−1073

http://pubs.acs.org/journal/acscii

Extraordinary Slowing of Structural Dynamics in Thin Films of a Room Temperature Ionic Liquid

Jun Nishida,[†,‡] John P. Breen,[†] Boning Wu, and Michael D. Fayer*

Department of Chemistry, Stanford University, Stanford, California 94305, United States

Supporting Information

ABSTRACT: The role that interfaces play in the dynamics of liquids is a fundamental scientific problem with vast importance in technological applications. From material science to biology, e.g., batteries to cell membranes, liquid properties at interfaces are frequently determinant in the nature of chemical processes. For most liquids, like water, the influence of an interface falls off on a ∼1 nm distance scale. Room temperature ionic liquids (RTILs) are a vast class of unusual liquids composed of complex cations and anions that are liquid salts at room temperature. They are unusual liquids with properties that can be finely tuned by selecting the structure of the cation and anion. RTILs are being used or developed in applications such as batteries, CO_2 capture, and liquids for biological processes. Here, it is demonstrated quantitatively that the influence of an interface on RTIL properties is profoundly different from that observed in other classes of liquids. The dynamics of planar thin films of the room temperature ionic liquid, 1-butyl-3-methylimidazolium bis(trifluoromethylsulfonyl)imide ($BmimNTf_2$), were investigated using two-dimensional infrared spectroscopy (2D IR) with the CN stretch of $SeCN^-$ as the vibrational probe. The structural dynamics (spectral diffusion) of the thin films with controlled nanometer thicknesses were measured and compared to the dynamics of the bulk liquid. The samples were prepared by spin coating the RTIL, together with the vibrational probe, onto a surface functionalized with an ionic monolayer that mimics the structure of the $BmimNTf_2$. Near-Brewster's angle reflection pump−probe geometry 2D IR facilitated the detection of the exceedingly small signals from the films, some of which were only 14 nm thick. Even in quarter micron (250 nm) thick films, the observed dynamics were much slower than those of the bulk liquid. Using a new theoretical description, the correlation length (exponential falloff of the influence of the interfaces) was found to be 28 ± 5 nm. This very long correlation length, ∼30 times greater than that of water, has major implications for the use of RTILs in devices and other applications.

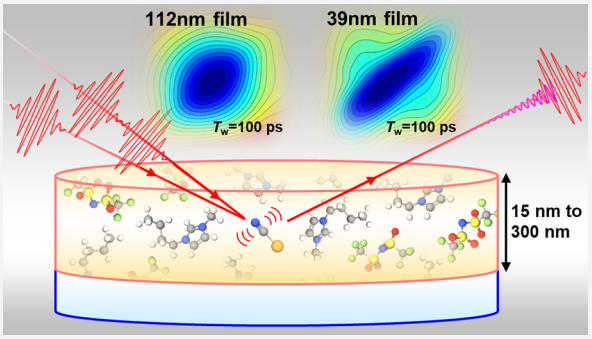

I. INTRODUCTION

Liquids at interfaces occur in a wide variety of chemical and biological systems. Molecules in a liquid in contact with an interface will have distinct properties from those in the bulk liquid. The structure and dynamics of liquid molecules at an interface and for some distance beyond the layer in direct contact with an interface are distinct from those of the bulk liquid. The structural and dynamical properties of molecules at an active interface, e.g., a battery electrode or a cell membrane, can be intimately involved in chemical processes.

Molecules in an interfacial layer will see the interface material on one side and the liquid molecules on the other. The molecules at the interface, which will not have bulk properties, i.e., structural organization and dynamics, will affect the next layer of molecules further from the interface, which in turn will affect the next layer. Generally, the influence of an interface dies off rapidly. After several liquid layers, typically on a distance scale of one to several nanometers, the influence of the interface is no longer present. Molecules at interfaces typically exhibit slower structural dynamics than those in bulk liquids.[1−3] Thus, the measurement of the dynamical time scales provides a useful approach for quantifying the influence of an interface and the length scale over which the interfacial perturbation propagates. For example, in the case of water molecules confined in sodium bis(2-ethylhexyl) sulfosuccinate (AOT) reverse micelles, the dynamics of water molecules located within ∼2 nm from the interfaces are significantly altered, slowing substantially; however, water molecules further away from the interface behave like those in bulk water.[4] Similar length scales have been reported in other liquid/interface systems.[5,6]

Room temperature ionic liquids (RTILs) are generally composed of organic cations and inorganic anions.[7,8] RTILs can be highly structured, even on mesoscopic distance scales, due to the Coulomb, van der Waals, and hydrogen-bonding interactions among the bulky ions. RTILs are being used or investigated for a wide variety of applications.[9] In many of these applications, such as electrolytes in batteries,[10,11] solvents for CO_2 capture in supported ionic liquid membranes,[12−14]

Received: June 4, 2018
Published: July 30, 2018

DOI: 10.1021/acscentsci.8b00353
ACS Cent. Sci. 2018, 4, 1065−1073

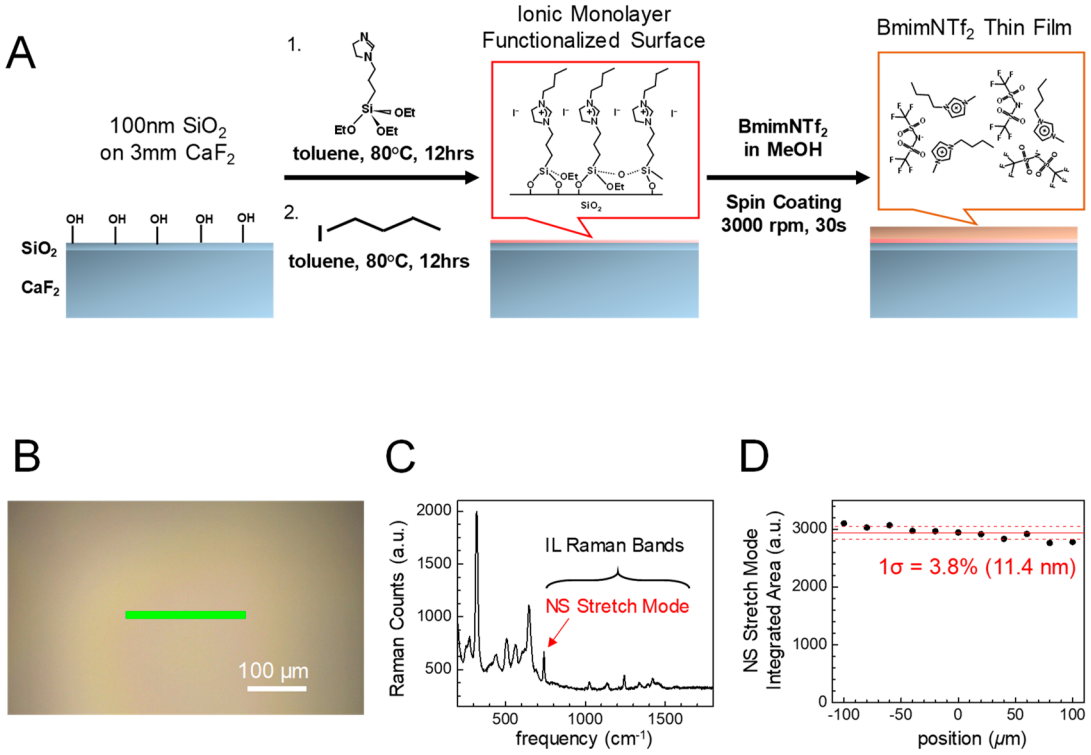

Figure 1. (A) Preparation procedure for $BmimNTf_2$ RTIL thin films. An SiO_2 surface is first functionalized with an ionic monolayer that mimics the structure of $BmimNTf_2$ RTIL. $BmimNTf_2$ dissolved in methanol is then spin coated onto the functionalized surface. For 2D IR measurements, BmimSeCN was mixed with $BmimNTf_2$ with 1:10 ratio as a vibrational probe. (B) Optical microscope image of ∼301 nm thick $BmimNTf_2$ film. (C) Micro-Raman spectrum acquired at the center of the image with 100× objective. The features above >700 cm^{-1} arise from the $BmimNTf_2$ RTIL. The particularly strong band at ∼740 cm^{-1} is assigned to the NS stretch mode of the NTf_2 anion. (D) Variation of the NS stretch Raman band intensity across the green horizontal line in part B, indicating that the RTIL film thickness is reasonably constant across the 200 μm range.

and media for biological studies,[15,16] the RTILs will be in contact with interfaces or confined on nanometer to submicron length scales.

Recently there have been qualitative reports that indicate RTILs may display the effect of interfaces on distance scales much longer than those found in other types of liquids, with estimated length scales varying from 60 to 2000 nm depending on the types of the RTILs and the interface.[17−20] A molecular dynamics (MD) simulation by Voth and co-workers indeed showed long-range structural ordering of alkylmethylimidazolium-based ionic liquids at the liquid/vacuum interface.[21] Particularly for the longer-chain cations, the interfacial structural ordering was found to persist beyond ∼10 nm from the interface. A recent MD simulation by Margulis and co-workers also revealed that 1-methyl-3-octylimidazolium octylsulfate can form a lamellar structure at the liquid/vacuum interface, and the structure extends to the full length scale of their simulation box (9 nm).[22]

The dynamics of RTILs in confined environments have also been studied recently. Shin et al. investigated the RTIL 1-ethyl-3-methylimidazolium bis(trifluoromethylsulfonyl)imide ($EmimNTf_2$) in the pores of poly(ether sulfone) (PES) membranes using ultrafast infrared techniques.[23,24] In spite of the large pore, 350 nm diameter on average,[25] the observed structural dynamics of the RTIL slowed in the pores compared to the bulk liquid. Thomaz et al. used time-dependent fluorescent Stokes shift measurements to study the dynamics of the alkylmethylimidazolium bis(trifluoromethylsulfonyl)-imide ($C_nmimNTf_2$) confined in the same membrane, with varying cation alkyl chain lengths.[26] Substantial slowing of the dynamics was again observed in the pores, with larger impacts on the RTILs with shorter alkyl chains. These measurements clearly demonstrate that the effects of the interfaces on dynamics propagate over much longer distance scales in the RTILs than in other liquids. However, the very broad distribution of the pore sizes (100−500 nm) and the complicated topography of the pores hindered the quantitative evaluation of distance scales.

In this paper we present two-dimensional infrared (2D IR) spectroscopy studies on planar thin films of the RTIL 1-butyl-3-methylimidazolium bis(trifluoromethylsulfonyl)imide ($BmimNTf_2$). The CN stretch of $SeCN^-$, introduced into the RTIL as BmimSeCN, was used as the vibrational probe because of its strong transition dipole moment and long vibrational lifetime.[27] The recently developed method of 2D IR spectroscopy in the near-Brewster's angle reflection pump−probe geometry facilitated the detection of the small signals from the thin films.[28] Films with the controlled thicknesses from 14 to 278 nm were investigated. In contrast to the experiments in the PES membranes, the films have well-defined thicknesses and topography, making it possible to obtain a quantitative evaluation of the distances over which the interfaces influence the dynamics of the RTIL. The 2D IR experiments showed that even quarter micron thick films exhibited dynamics that were significantly slower than the bulk liquid. As the films were made thinner, the dynamics slowed dramatically.

DOI: 10.1021/acscentsci.8b00353
ACS Cent. Sci. 2018, 4, 1065−1073

II. PREPARATION OF THE RTIL THIN FILMS

Several publications have reported the coating or deposition of ionic liquids on flat dielectric and metallic surfaces.[29−35] In many of these studies, the focus was on the formation of nanodroplets of RTILs,[31,32,34] rather than planar films of RTILs of interest here. Successful preparation of the ionic liquid thin films has been reported using ultrahigh vacuum physical vapor deposition (UHV-PVD) methods,[30,35] requiring complex apparatus that is not widely available.

Spin coating is a well-established method for preparing thin films. Spin coating $BmimNTf_2$ RTIL directly onto an SiO_2 surface using the RTIL dissolved in methanol yielded droplets rather than a planar film, as seen in the microscope optical image shown in Figure S1 (see the Supporting Information). This result showed that the affinity between the $BmimNTf_2$ RTIL and the SiO_2 surface is not high enough to overcome the surface tension, preventing the formation of an extended planar film.

To enhance the affinity between the $BmimNTf_2$ RTIL and the interface, the SiO_2 surface was functionalized with an ionic monolayer that mimics the structure of $BmimNTf_2$ (Figure 1A) by adapting a procedure reported by Xin and Hao.[36] Spin coating of $BmimNTf_2$ RTIL on the functionalized surface yielded a film with high optical quality, as seen in the microscope images (Figure 1B) acquired with a Raman microscope (Horiba XploRA). Micro-Raman spectra acquired at spatial points along the green line in Figure 1B clearly show the strong NS stretching mode originating from NTf_2^- anion (Figure 1C).[37] The intensity of the NS stretch band at each point is plotted in Figure 1D, demonstrating that the thickness of the film formed is reasonably uniform. The fractional variation increased as the film thickness was decreased. The influence of variations in film thickness within the laser spot is analyzed quantitatively below. It is shown that the variation does not change the results obtained from analysis of the 2D IR experiments as the observed dynamics are essentially determined by the averaged thickness. It is worth noting that the thickness of the functionalized SiO_2 ionic monolayer (∼1 nm) is significantly thinner than any of the RTIL films (14−300 nm).

The thickness of the spin coated films was controlled by the concentration of the RTIL in the precursor methanol solution. To introduce the $SeCN^-$ anion as the vibrational probe for the 2D IR spectroscopy, BmimSeCN was mixed with $BmimNTf_2$ in a 1:10 molar ratio. BmimSeCN only minutely perturbs the dynamics of $BmimNTf_2$ RTIL (Figure S2). The thicknesses of the spin coated films were characterized with FTIR absorption spectra by comparing the peak heights of the CH stretching modes of the $Bmim^+$ cation with those of the bulk $BmimNTf_2$ liquid with a known thickness (Figure S3). Further details on the sample preparation and characterization can be found in the Supporting Information. All spin coating was conducted in a nitrogen-filled glovebox. The samples were then sealed in airtight sample cells in the glovebox. Thus, the samples were not exposed to either atmospheric humidity or oxygen.

III. RESULTS AND DISCUSSION

A. Linear Spectra. The normalized FTIR spectra of the CN stretch of $SeCN^-$ in bulk $BmimNTf_2$ and in films with thickness of 278, 112, and 39 nm are shown in Figure 2. The 39 nm film, for example, has a CN absorbance of only 1 mOD. The peak center positions and the line widths for Gaussian fits

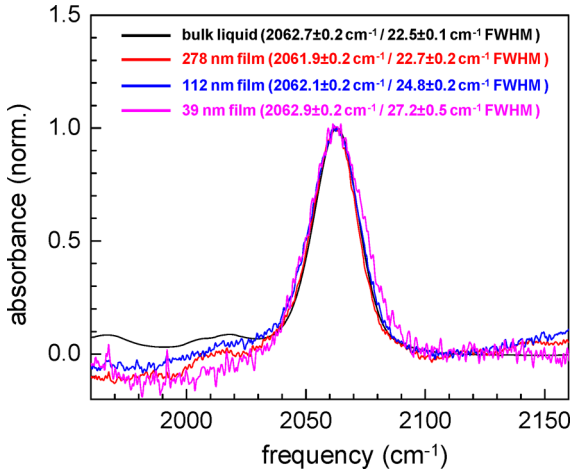

Figure 2. FTIR spectrum of $SeCN^-$ anion dissolved in $BmimNTf_2$ films with different thickness. The peak positions and full width at half-maximum derived based on Gaussian fits are given. The peak positions are independent of the film thickness, while the bandwidth may be broader in ∼39 nm film by up to 20% compared with the bulk solution. Although the absorption bands are almost identical, the dynamics in the films strongly depend on their thickness.

are given in Figure 2. All of the bands have the same center position within experimental error, 2062.5 ± 0.5 cm^{-1}. The bulk and 278 nm film spectra have the same fwhm within error, 22.6 cm^{-1}. The fits give an increasing fwhm for the thinner films, 24.8 and 27.2 cm^{-1}, for the 112 and 39 nm films, respectively. Imperfect baseline subtractions can produce systematic error, which might be responsible for the different line widths. The same measurement was applied to the thinnest 14 nm film as well. Though the data are not included in Figure 2, the fit to the 14 nm film yielded a fwhm width of ∼25.5 cm^{-1}. Though the line width may be increasing as the film thickness is reduced (by up to 20% in the 39 nm film compared with the bulk liquid), overall the peak positions and line widths in the films are not substantially altered from those of the bulk liquid. As discussed below, in spite of the lack of substantial differences in the linear absorption spectra, the dynamics of the films are very different from those of the bulk liquid and depend strongly on thickness.

B. 2D IR Spectroscopy on the RTIL Thin Films. As seen in Figure 2, the infrared absorption band of the $SeCN^-$ anions has a finite bandwidth. The width, i.e., the variation of the CN stretch vibrational frequency (inhomogeneous broadening), arises from different RTIL structural configurations, which cause distinct interactions between the $SeCN^-$ anions and their surroundings. The RTIL undergoes structural fluctuations, inducing the CN frequencies to change with time. At sufficiently long time, each CN will sample all frequencies throughout the inhomogeneous line's range of frequencies. Thus, measuring the time evolution of the vibrational frequencies (spectral diffusion) reports directly on the RTIL structural dynamics.

Two-dimensional IR spectroscopy characterizes the spectral diffusion by making a correlation plot between the initial and the final frequencies.[38−41] The measurements of the initial and final frequencies are separated by a waiting time T_w (Figure 3). As seen in Figure 3A,B, 2D IR spectroscopy involves three input pulses. The first two "pump" pulses together label the initial frequencies (2D spectrum horizontal axis ω_τ), and after the time T_w, the third "probe" pulse initiates the emission of

DOI: 10.1021/acscentsci.8b00353
ACS Cent. Sci. 2018, 4, 1065−1073

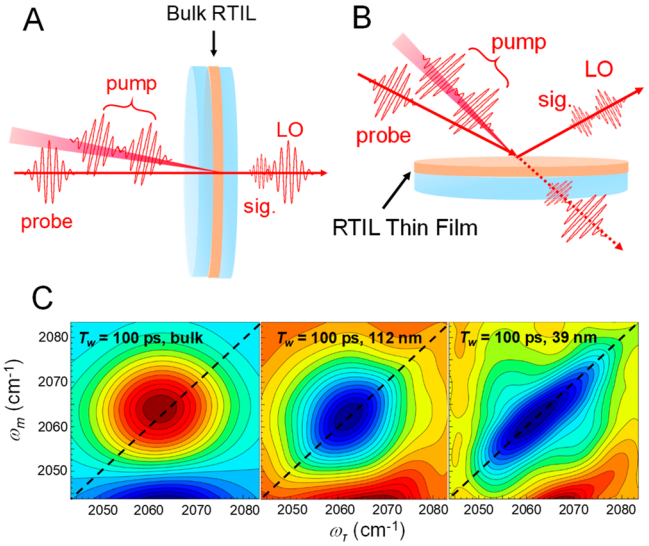

Figure 3. (A) Two-dimensional IR spectroscopy for bulk liquid samples implemented in the standard transmission pump−probe geometry. The first two "pump" pulses label the initial frequencies, and after a waiting time T_w, the third "probe" pulse induces the emission of the vibrational echo signal, which reads out the final frequencies. The emitted signal field interferes with the transmitted probe pulse as a local oscillator, and the amplitude of the interference is recorded as the signal. (B) Two-dimensional IR spectroscopy implemented in the near-Brewster's angle reflection pump−probe geometry for ionic liquid thin films. The two pump pulses and the probe pulse play the identical roles as in the standard geometry. The emitted signal field interferes with the heavily attenuated reflected probe field, which enhances the signal to local oscillator ratio, greatly improving the detection. (C) Two-dimensional IR spectra for the bulk $BmimNTf_2$ and two films with the thickness of 112 and 39 nm, acquired at the waiting time T_w = 100 ps. More correlated band shapes in the thinner films indicate slower structural dynamics.

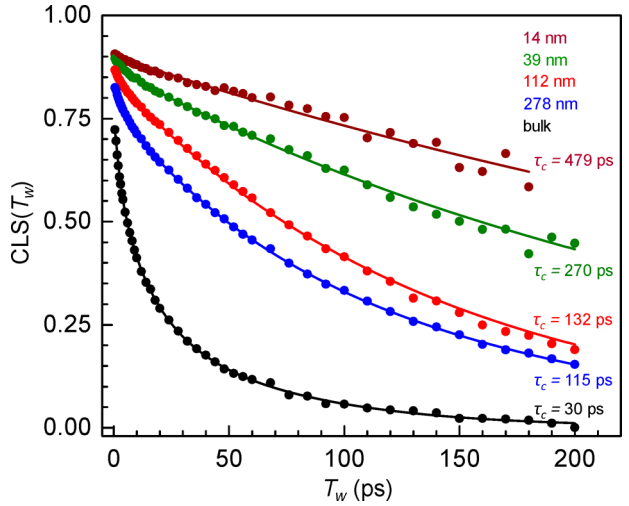

Figure 4. Center line slope (CLS) decays extracted from T_w-dependent 2D IR band shapes for films with different thicknesses (14, 39, 112, and 278 nm, and bulk). Each decay curve is the average of data taken on several independently prepared samples. Dots − averaged data. Lines − fits to multiexponential decays, with time constants given in Table 1. The time constants shown next to each curve are correlation times calculated based on the fits. As the films become thinner, the dynamics slow dramatically.

the vibrational echo pulse, which reads out the final frequencies (vertical axis, ω_m). If T_w is small compared with the dynamical time scales of the system, the initial and the final frequencies will be similar and yield a diagonally elongated band shape. In contrast, when T_w is sufficiently large, the structural fluctuations during the waiting time substantially randomize the vibrational frequencies, and the initial and final frequencies lose correlation, yielding a more rounded band shape.

Figure 3C shows 2D IR spectra for three samples at a single waiting time, T_w = 100 ps. The signs of the 2D IR band shapes are different between the bulk sample and the thin films because they were measured in different geometries as shown in Figure 3A (the transmission geometry for the bulk liquid sample) and Figure 3B (the reflection geometry for films).[28] The bulk spectrum is nearly round, indicating the structural fluctuations in the bulk RTIL during the 100 ps between the labeling and reading have almost randomized the vibrational frequency. The nearly round shape shows that almost all of the structural configurations that give rise to the inhomogeneously broadened line have been sampled in 100 ps. In contrast, the spectrum of the 112 nm film is elongated along the diagonal, and the 39 nm sample is substantially more elongated. That is, during the 100 ps, the vibrational frequencies were not significantly altered, demonstrating that the structural fluctuations in the thin films occur on much slower time scales than that of the bulk RTIL. It is qualitatively clear that the thinner films exhibit slower dynamics.

C. Center Line Slope (CLS) Decays and Spectral Diffusion Time Constants. The dynamical time constants are obtained by evaluating the evolving band shapes of the 2D spectra with increasing T_w. The T_w-dependent changes in the band shapes can be analyzed quantitatively using the center line slope (CLS) method.[42,43] The CLS(T_w) decay is the normalized frequency−frequency correlation function (FFCF).[42,43] Figure 4 shows the CLS decays for each sample. As the sample becomes thinner, there is a dramatic slowing of the decay, reflecting a slowing of the structural dynamics of the sample.

The solid curves through the data are multiexponential fits, with the fitting time constants given in Table 1. Both the bulk sample and the 278 nm film were fit well with the same functional form (a triexponential), and both decay close enough to zero and have sufficient slope that it is reasonable to assume that there is no slower component that cannot be observed in the 200 ps limit on the data collection due to the vibrational lifetime.

For the bulk sample and the 278 nm films, the three time constants, τ_1, τ_2, and τ_3, are given in Table 1 and can be directly compared. The three time constants reflect time scales for different types of structural dynamics. The dynamics on all three time scales slow substantially, by factors of ∼2 to ∼3, in the 278 nm films compared with the bulk liquid. These results show the dramatic slowing of the dynamics in the film even though the film is approximately a quarter of a micron thick.

While the bulk data and the 278 nm film data fit extremely well to triexponential fits, fits to the CLS decays for the other three film thicknesses (112, 39, and 14 nm) are biexponentials. For fitting purposes, it was assumed that the slower component of each curve decays to zero (see further discussion below). The fit time constants are τ_1 and τ_2 in Table 1. In the biexponential fits to these three thinner films, the slower time constants (τ_2) were slower than τ_2 in the bulk liquid and 278

DOI: 10.1021/acscentsci.8b00353
ACS Cent. Sci. 2018, 4, 1065−1073

Table 1. CLS Parameters from Fits

sample	T_w = 0 value[a]	τ_1 (ps)	τ_2 (ps)	τ_3 (ps)	τ_c (ps)	normalized CLS[b] at T_w = 150 ps
bulk liquid	0.76	2.5 ± 1	15 ± 2	62 ± 3	30 ± 1	0.03
278 nm	0.84	5.0 ± 0.7	46 ± 17	136 ± 8	115 ± 7	0.27
112 nm	0.88	2.0 ± 0.6	136 ± 2		132 ± 2	0.32
39 nm	0.90	3.8 ± 2	278 ± 7		270 ± 7	0.57
14 nm	0.91	4.0 ± 1.2	484 ± 14		479 ± 10	0.73

[a]The difference between the T_w = 0 value and 1 is directly related to the homogeneous line width. The closer the value is to 1, the narrower the homogeneous line width. [b]The value of the CLS at 150 ps after the curves have been normalized to 1 at T_w = 0 ps to eliminate the differences caused by the varying homogenous line widths..

nm film, and as the thickness was reduced τ_2 slowed substantially. This behavior is in accordance with the general behavior observed so far; i.e., the thinner films exhibit increasingly slower dynamics. In contrast, the faster component (τ_1) is faster than the fastest component τ_1 observed in the 278 nm film (see Table 1). One possibility that can explain this seemingly anomalous behavior is a substantial slowing of some of the dynamical components that are responsible for the ultrafast fluctuations that contribute to motional narrowing in the bulk liquid. Motional narrowing occurs when $\Delta \times \tau < 1$, where Δ is the range of the frequency fluctuations, and τ is the time for sampling these frequencies.[38,42,44] The motionally narrowed dynamical component contributes to the Lorentzian-shaped homogeneous line width in the linear absorption spectrum, and reduces the CLS value at T_w = 0 ps from 1 in the 2D spectrum; the motionally narrowed component does not contribute to the CLS decay. As is evident from Figure 4, the CLS value at T_w = 0 ps increases as the thickness is reduced, indicating that the homogeneous line width has decreased. It is likely that some of the homogeneous line width is converted to inhomogeneous line width as τ slows, and consequently, $\Delta \times \tau < 1$ is no longer satisfied. The new inhomogeneous component will undergo fast spectral diffusion as originally it experienced faster fluctuations that caused motional narrowing. The result is the fast τ_1s and smaller homogeneous line widths in the three thinnest films.

To compare all samples, in spite of the fact that they do not fit to the same functional form, the correlation times τ_c (the time integrals of the normalized decays) were calculated assuming the slowest component of each curve decayed to zero. Due to the observable time range, limited by the vibrational lifetime of the vibrational probe (~100 ps), we could not exclude the possibility that even slower dynamics exist in the thinner films. The correlation times for the thinner films listed in Table 1 and on Figure 4 should therefore be regarded as lower bounds.

D. Origin of the Observed Dynamical Slowing. Before discussing quantitatively the thickness dependence of the thin films' structural dynamics, it is illuminating to consider the possible physical mechanisms of the observed dynamical slowing. An MD simulation by Del Pópolo and Voth provides important insights.[45] Based on the physical picture from their MD simulation, the $SeCN^-$ anion vibrational probe is trapped in a "long-lived cage" formed by the surrounding cations and anions. The dynamics on faster time scales (<10 ps) may arise from very local motions of the cage and the $SeCN^-$ anions. The dynamics occurring on slower time scales (>100 ps) are associated with longer distance scale structural evolution that structurally relaxes the cages.

As seen in Figure 4 and Table 1, the dynamics of the thinner films are characterized by the emergence of extremely slow dynamics (≫100 ps), demonstrating that the influence of the interfaces persists for much longer times. The interfaces impose global structural and/or dynamical ordering through long-range Coulomb interactions, which result in the extensive length scale of the "cages" surrounding individual cations and anions.

The dynamical slowing in supercooled liquids near glass transition temperatures (T_g) has often been discussed in a similar manner, i.e., the growing dynamical correlation lengths of cooperatively rearranging regions as the liquids are cooled toward T_g.[46−50] In this sense, the dynamical behavior of ionic liquid molecules at the interfaces may resemble that of a supercooled liquid near T_g. The observations here might provide insights into the behavior of supercooled liquids under confinement.[51,52]

E. Quantifying the Correlation Length. A main interest here is the quantitative determination of the correlation length, i.e., the length scale over which the interfaces affect the dynamics of the RTIL molecules. Instead of the correlation times discussed above, which have ambiguity due to the limited observable time range, we define and evaluate the correlation length based on the values of the normalized CLS decays at T_w = 150 ps, which have well-defined values for all of the decays in Figure 4. The values are listed in Table 1 and plotted in Figure 5A. The decays were normalized to eliminate the influence of varying CLS values at T_w = 0 ps (given in Table 1) originating from varying homogeneous line widths. The value of T_w = 150 ps was selected because of the pronounced differences among the curves and good S/N ratios.

Figure 5B shows a schematic illustration of the RTIL film and the dynamical behavior at each location inside the film. The interfaces are separated by a distance, d. Far enough from the interface, the system will have bulk dynamics. Near the interface, the dynamics are slower. As a result, the frequency−frequency correlation function (FFCF) at T_w = 150 ps, $f(r, T_w = 150\ \text{ps})$, varies within the film depending on the distance r from the interface. We assume that the influence of the interface falls off exponentially with the distance, r, from the interface. Then the dependence is described by

$$f(r, T_w) = [f_0(T_w) - f_b(T_w)] \exp(-r/l) + f_b(T_w) \quad (1)$$

where the waiting time T_w here is 150 ps, and $f_0(T_w)$ and $f_b(T_w)$ are the frequency−frequency correlation functions of a thin slab at the interface (r = 0) and in the bulk region ($r \to \infty$), respectively. In this model, the characteristic length scale of the interfacial influence is specified by the correlation length l, which describes the exponential falloff of the interfacial effect as the distance r from the interface is increased.

In the 2D IR measurements, all of the molecules inside a film contribute to the signal, and therefore the data reflect the

DOI: 10.1021/acscentsci.8b00353
ACS Cent. Sci. 2018, 4, 1065−1073

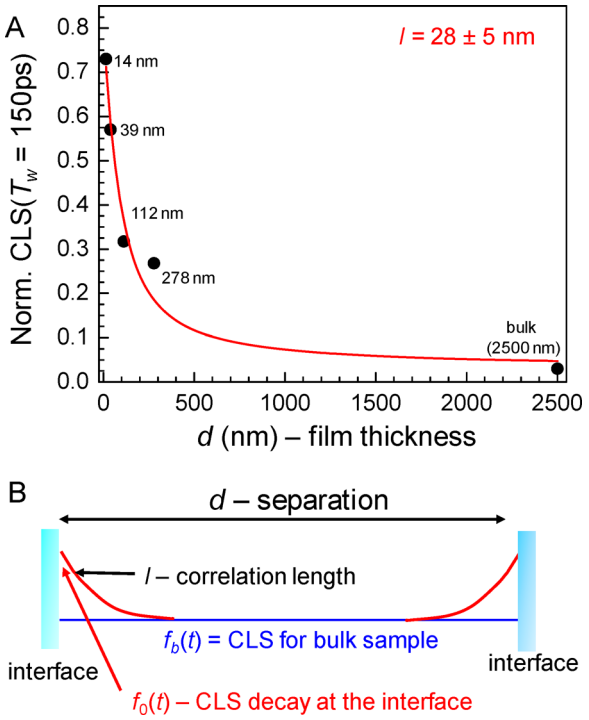

Figure 5. (A) Normalized CLS values at T_w = 150 ps plotted vs the film thickness. Dots − averaged data. Red line − the fit of the data to eq 2, yielding the correlation length of 28 ± 5 nm. (B) Schematic illustration of the interfacial effect on the dynamics of the RTIL molecules confined in the film. In a thin slab at the surfaces, the dynamics are very slow, and thus the FFCF at a certain time has a high value. Far enough away from the interfaces, molecules cannot sense the presence of the interfaces, and thus the FFCF is identical to that of the bulk solution. The correlation length l describes the exponential falloff of the interfacial effect with respect to the distance from the interfaces.

average (integral) over r. If the thickness d is very large, the measurements give the bulk RTIL dynamics, because the fraction of the volume that is perturbed by the interfaces is negligible. However, when d is only a few correlation lengths, a substantial fraction or all of the volume will have nonbulk dynamics, and the 2D IR results will differ from those of the bulk. To calculate the experimentally observed dynamics as a function of the film thickness, it is necessary to integrate eq 1 over r.

$$f_{obs}(d, T_w) = (2/d)[f_0(T_w) - f_b(T_w)]\int_0^{d/2} \exp(-r/l)\, dr + (2/d)\int_0^{d/2} f_b(T_w)\, dr \quad (2)$$

For simplicity, the influence of the two interfaces is taken to be the same, so the integral is performed from 0 to $d/2$. The term $(2/d)$ is the normalization constant. The integration of eq 1 over r yields the observed FFCF, $f_{obs}(d, T_w)$, for a film with thickness d given by

$$f_{obs}(d, T_w) = (2/d)[f_0(T_w) - f_b(T_w)][l(1 - \exp(-d/2l))] + f_b(T_w) \quad (3)$$

Again, here, T_w is set to 150 ps. As the observed normalized CLS is proportional to the FFCF, the data in Figure 5A can be fit with eq 3.

The red curve in Figure 5A is the fit, which yields the correlation length l = 28 ± 5 nm. The equivalent correlation length for water molecules confined in AOT reverse micelles has been estimated to be ∼1 nm, and thus the correlation length obtained here for the RTIL films is roughly 30 times longer. The value of l is consistent with the fact that even a sample that is 278 nm thick displays dynamics that differ significantly from bulk dynamics. For d = 278 nm, the center of the sample, $d/2$, is ∼139 nm from the interfaces, which is <5l. Most of the sample volume will feel the influence of the interfaces.

Note that, in the theoretical model, the influences of the two different surfaces (ionic monolayer surface and 1 atm nitrogen gas) on the RTIL were assumed identical. While the solid surface is functionalized with cations, the previous molecular dynamics simulation demonstrated that RTIL/vacuum interfaces should also be cation-rich.[22] Therefore, the correlation lengths imposed by these two interfaces might be similar. The single 28 nm correlation length obtained here should be regarded as the "average" correlation length originating from these two interfaces.

F. Effect of Thickness Variation. As discussed in the Supporting Information, measurements using Raman microscopy show that there are fluctuations in the thickness as a function of position across the film. For the thin samples, the standard deviation of the range of thicknesses can become large, and even for the thicker samples, the variation is not negligible. However, the variations occur over short distances. The laser spot size that gives rise to most of the signal is ∼180 μm in diameter, which is large compared to the distances over which the thickness variations are observed (<10 μm). Therefore, the observed signal is the average over the thickness variation. It is important to address how much the variation in thickness within the laser spot will affect the observed results for various film average thicknesses, d_{ave}.

To address the influence of thickness fluctuations within the laser spot area, we can begin with eq 3. It is necessary to integrate eq 3 over the variations in d for a particular average value of d_{ave}. The probability distribution of the thickness, $P(d)$, is taken to be Gaussian with a standard deviation σ about the average thickness, d_{ave}, for a given sample. In addition, the signal varies linearly in d. A thicker region of the sample within the laser spot will give more signal. To account for this, there is an additional multiplicative factor, d/d_{ave}.

$$f_{ave}(T_w) = \int_{-\infty}^{\infty} (2/d)(d/d_{ave})[f_0(T_w) - f_b(T_w)][l(1 - \exp(-d/2l))]P(d)\, dd + f_b(T_w) \quad (4)$$

Then for a normalized Gaussian distribution

$$f_{ave}(T_w) = \frac{2l[f_0(T_w) - f_b(T_w)]}{d_{ave}\sqrt{2\pi\sigma^2}}\int_{-\infty}^{\infty}[1 - \exp(-d/2l)]\exp(-(d - d_{ave})^2/2\sigma^2)\, dd + f_b(T_w) \quad (5)$$

The result of the integration is

$$f_{ave}(T_w) = \frac{2l[f_0(T_w) - f_b(T_w)]}{d_{ave}}[1 - \exp(-((d_{ave}/2l) - (\sigma^2/8l^2)))] + f_b(T_w) \quad (6)$$

Equation 6 is a useful result. It is the same as eq 3 except for the extra term in the exponential, $(\sigma^2/8l^2)$. To determine the

DOI: 10.1021/acscentsci.8b00353
ACS Cent. Sci. 2018, 4, 1065−1073

influence of thickness variation within the laser spot, we need to compare the magnitude of $\sigma^2/8l^2$ to the other term in the exponential, $d_{ave}/2l$. From the fit shown in Figure 5A, the correlation length is l = 28 nm. For the thickest sample, d_{ave} = 280 nm, and $d_{ave}/2l$ = 5. For this sample thickness, the typical standard deviation is about 0.1 of the thickness, $\sigma = 0.1d_{ave}$. Then the additional term in the exponential is 0.125, which is negligible compared to $d_{ave}/2l$ = 5. The thinnest sample has a much larger fractional variation. For the thinnest sample, d_{ave} = 14 nm, and $d_{ave}/2l$ = 0.25. $\sigma \sim 0.4d_{ave}$ (see the Supporting Information). Then the extra term in the exponential is 5×10^{-3}, which is negligible compared to 0.25. The net result is that the variation in thickness within the laser spot size does not affect the estimation of the correlation length which was based on the average thickness, d_{ave}.

IV. CONCLUDING REMARKS

Liquid molecules in contact with an interface will always have properties that are different from those of the bulk liquid. The distinct intermolecular interactions between the interface and the liquid molecules and the topography of the interfacial layer will cause the liquid contact layer to have different structural and dynamical properties from those of the bulk liquid. For most liquids, after a few molecular diameters (1-2 nm) from the interface, the liquid's intermolecular interactions will overcome the influence of the distinct interface−molecule interactions, and the liquid will have bulk properties. However, these trends may not apply when the liquids in question are room temperature ionic liquids. In this study we have shown quantitatively that an ionic liquid can have nonbulk properties far from an interface. The difference between the behavior of conventional liquids and RTILs is presumably caused by the strong Coulomb interactions among the complex cations and anions that comprise the RTIL.

To investigate the influence of interfaces on RTILs, we have presented a detailed study of thin films of $BmimNTf_2$. The RTIL was spin coated onto a surface functionalized with an ionic monolayer, the structure of which resembles that of the $Bmim^+$ cation. The structural dynamics of the films were studied by measuring spectral diffusion using 2D IR spectroscopy on a vibrational probe, $SeCN^-$, dissolved in the films. The film thickness ranged from 14 to 278 nm. Measurements on the films were compared to measurements on the same RTIL bulk liquid.

The structural dynamics of the films were found to be substantially slower than those of the bulk liquid, even for the 278 nm thick films. Based on the correlation times obtained from the observed spectral diffusion dynamics, the thinnest 14 nm film exhibited dynamics that are at least 15 times slower than those of the bulk liquid. A model was developed to quantify the substantial slowing of the dynamics as the films become thinner. Fitting the data in Figure 5A with eq 3, the correlation length l was found to be 28 ± 5 nm. The correlation length can be regarded as the length scale over which the influences of the interfaces fall off exponentially. Any interface will have interactions with the liquid molecules that are different from interactions among the molecules themselves. Here, the solid interface is functionalized with cations, and it is likely that the RTIL/air interface is also cation-rich based on MD simulation studies.[22] With cation-rich interfaces, the anion solvation will be very different from the bulk liquid, substantially perturbing the ionic structure. This modification of the ion−ion arrangement will propagate far out from the interfaces because of the long-range Coulomb interactions.

The study presented here raises a large number of questions. What effect will the length of cation alkyl chains have on the correlation length? What is the role of the interface properties, e.g., replacing a cationic functionalized interfacial layer with a nonionic but polar layer? How will changing the ions influence the correlation length, for example, replacing NTf_2^- with BF_4^-? The slowing of the dynamics of the RTIL induced by a well-defined interface, as reported here, can serve as a benchmark for understanding interfacial effects on RTILs. The results also have implications for interfacial processes, such as the diffusion of ions to a battery electrode, and for possible control of interfacial boundary layer properties by tailoring the nature of the interface and the choice of RTIL.

■ ASSOCIATED CONTENT

Supporting Information

The Supporting Information is available free of charge on the ACS Publications website at DOI: 10.1021/acscentsci.8b00353.

Sample preparation procedure, thickness characterization by FTIR absorption spectra, optical images and Raman microscopy, and ultrafast infrared laser system (PDF)

■ AUTHOR INFORMATION

Corresponding Author

*E-mail: fayer@stanford.edu. Phone: 650 723-4446.

ORCID

Jun Nishida: 0000-0001-7834-8179
Boning Wu: 0000-0003-2280-3448
Michael D. Fayer: 0000-0002-0021-1815

Present Address

‡J.N.: Department of Physics, Department of Chemistry, and JILA, University of Colorado Boulder, Boulder, Colorado 80309, United States.

Author Contributions

†J.N. and J.P.B. contributed equally to the work.

Notes

The authors declare no competing financial interest.
Safety Statement: no unexpected or unusually high safety hazards were encountered.

■ ACKNOWLEDGMENTS

This work was supported by the Air Force Office of Scientific Research Grant FA9550-16-1-0104 (J.N., B.W., and M.D.F. and instrumentation), by the Division of Chemical Sciences, Geosciences, and Biosciences, Office of Basic Energy Sciences of the U.S. Department of Energy (DOE) Grant DEFG03-84ER13251 (J.P.B., B.W., and M.D.F.). Part of this work was performed at the Stanford Nano Shared Facilities (SNSF), supported by the National Science Foundation under award ECCS-1542152.

■ REFERENCES

(1) Singh, P. C.; Nihonyanagi, S.; Yamaguchi, S.; Tahara, T. Ultrafast Vibrational Dynamics of Water at a Charged Interface Revealed by Two-Dimensional Heterodyne-Detected Vibrational Sum Frequency Generation. *J. Chem. Phys.* **2012**, *137* (9), 094706.

DOI: 10.1021/acscentsci.8b00353
ACS Cent. Sci. 2018, 4, 1065−1073

(2) Hsieh, C. S.; Okuno, M.; Hunger, J.; Backus, E. H.; Nagata, Y.; Bonn, M. Aqueous Heterogeneity at the Air/Water Interface Revealed by 2D-HD-SFG Spectroscopy. *Angew. Chem. Int. Ed.* **2014**, *53* (31), 8146.
(3) Yan, C.; Thomaz, J. E.; Wang, Y.-L.; Nishida, J.; Yuan, R.; Breen, J. P.; Fayer, M. D. Ultrafast to Ultraslow Dynamics of a Langmuir Monolayer at the Air/Water Interface Observed with Reflection Enhanced 2D IR Spectroscopy. *J. Am. Chem. Soc.* **2017**, *139* (46), 16518.
(4) Moilanen, D. E.; Fenn, E. E.; Wong, D.; Fayer, M. D. Water Dynamics in Large and Small Reverse Micelles: From Two Ensembles to Collective Behavior. *J. Chem. Phys.* **2009**, *131*, 014704.
(5) Coasne, B.; Fourkas, J. T. Structure and Dynamics of Benzene Confined in Silica Nanopores. *J. Phys. Chem. C* **2011**, *115*, 15471.
(6) Zhu, X.; Farrer, R. A.; Fourkas, J. T. Ultrafast Orientational Dynamics of Nanoconfined Benzene. *J. Phys. Chem. B* **2005**, *109*, 12724.
(7) Castner, E. W.; Margulis, C. J.; Maroncelli, M.; Wishart, J. F. Ionic Liquids: Structure and Photochemical Reactions. *Annu. Rev. Phys. Chem.* **2011**, *62* (1), 85.
(8) Hayes, R.; Warr, G. G.; Atkin, R. Structure and Nanostructure in Ionic Liquids. *Chem. Rev.* **2015**, *115* (13), 6357.
(9) Plechkova, N. V.; Seddon, K. R. Applications of Ionic Liquids in the Chemical Industry. *Chem. Soc. Rev.* **2008**, *37* (1), 123.
(10) Xue, L.; Tucker, T. G.; Angell, C. A. Ionic Liquid Redox Catholyte for High Energy Efficiency, Low-Cost Energy Storage. *Adv. Energy Mater.* **2015**, *5*, 1500271.
(11) Lin, M.-C.; Gong, M.; Lu, B.; Wu, Y.; Wang, D.-Y.; Guan, M.; Angell, M.; Chen, C.; Yang, J.; Hwang, B.-J.; et al. An Ultrafast Rechargeable Aluminium-Ion Battery. *Nature* **2015**, *520*, 324.
(12) Scovazzo, P.; Visser, A. E.; Davis, J. H.; Rogers, R. D.; Koval, C. A.; DuBois, D. L.; Noble, R. D. In *Ionic Liquids*; American Chemical Society: Washington D.C., 2002; Vol. *818*.
(13) Lozano, L. J.; Godínez, C.; de los Ríos, A. P.; Hernández-Fernández, F. J.; Sánchez-Segado, S.; Alguacil, F. J. Recent Advances in Supported Ionic Liquid Membrane Technology. *J. Membr. Sci.* **2011**, *376*, 1.
(14) Dai, Z.; Noble, R. D.; Gin, D. L.; Zhang, X.; Deng, L. Combination of Ionic Liquids with Membrane Technology: A New Approach for CO_2 Separation. *J. Membr. Sci.* **2016**, *497*, 1.
(15) Fujita, K.; MacFarlane, D. R.; Forsyth, M. Protein Solubilising and Stabilising Ionic Liquids. *Chem. Commun.* **2005**, 4804.
(16) Basu, A.; Bhattacharya, S. C.; Kumar, G. S. Influence of the Ionic Liquid 1-Butyl-3-Methylimidazolium Bromide on Amyloid Fibrillogenesis in Lysozyme: Evidence from Photophysical and Imaging Studies. *Int. J. Biol. Macromol.* **2018**, *107*, 2643.
(17) Parr, D.; Chrestenson, J.; Malik, K.; Molter, M.; Zibart, C.; Egan, B.; Haverhals, L. M. Structure and Dynamics at Ionic Liquid/Electrode Interfaces. *ECS Trans.* **2015**, *66* (30), 35.
(18) Jurado, L. A.; Kim, H.; Arcifa, A.; Rossi, A.; Leal, C.; Spencer, N. D.; Espinosa-Marzal, R. M. Irreversible Structural Change of a Dry Ionic Liquid under Nanoconfinement. *Phys. Chem. Chem. Phys.* **2015**, *17* (20), 13613.
(19) Anaredy, R. S.; Shaw, S. K. Long-Range Ordering of Ionic Liquid Fluid Films. *Langmuir* **2016**, *32* (20), 5147.
(20) Bou-Malham, I.; Bureau, L. Nanoconfined Ionic Liquids: Effect of Surface Charges on Flow and Molecular Layering. *Soft Matter* **2010**, *6* (17), 4062.
(21) Jiang, W.; Wang, Y.; Yan, T.; Voth, G. A. A Multiscale Coarse-Graining Study of the Liquid/Vacuum Interface of Room-Temperature Ionic Liquids with Alkyl Substituents of Different Lengths. *J. Phys. Chem. C* **2008**, *112* (4), 1132.
(22) Amith, W. D.; Hettige, J. J.; Castner, E. W.; Margulis, C. J. Structures of Ionic Liquids Having Both Anionic and Cationic Octyl Tails: Lamellar Vacuum Interface vs Sponge-Like Bulk Order. *J. Phys. Chem. Lett.* **2016**, *7* (19), 3785.
(23) Shin, J. Y.; Yamada, S. A.; Fayer, M. D. Dynamics of a Room Temperature Ionic Liquid in Supported Ionic Liquid Membranes Vs. The Bulk Liquid: 2D IR and Polarized IR Pump-Probe Experiments. *J. Am. Chem. Soc.* **2017**, *139*, 311.
(24) Shin, J. Y.; Yamada, S. A.; Fayer, M. D. Carbon Dioxide in a Supported Ionic Liquid Membrane: Structural and Rotational Dynamics Measured with 2D IR and Pump−Probe Experiments. *J. Am. Chem. Soc.* **2017**, *139*, 11222.
(25) Ramakrishnan, S.; McDonald, C.; Prud'homme, R.; Carbeck, J. Latex Composite Membranes: Structure and Properties of the Discriminating Layer. *J. Membr. Sci.* **2004**, *231* (1), 57.
(26) Thomaz, J. E.; Bailey, H. E.; Fayer, M. D. The Influence of Mesoscopic Confinement on the Dynamics of Imidazolium-Based Room Temperature Ionic Liquids in Polyether Sulfone Membranes. *J. Chem. Phys.* **2017**, *147*, 194502.
(27) Tamimi, A.; Fayer, M. D. Ionic Liquid Dynamics Measured with 2D IR and IR Pump−Probe Experiments on a Linear Anion and the Influence of Potassium Cations. *J. Phys. Chem. B* **2016**, *120* (26), 5842.
(28) Nishida, J.; Yan, C.; Fayer, M. D. Enhanced Nonlinear Spectroscopy for Monolayers and Thin Films in Near-Brewster's Angle Reflection Pump-Probe Geometry. *J. Chem. Phys.* **2017**, *146*, 094201.
(29) Carmichael, A. J.; Hardacre, C.; Holbrey, J. D.; Nieuwenhuyzen, M.; Seddon, K. R. Molecular Layering and Local Order in Thin Films of 1-Alkyl-3-Methylimidazolium Ionic Liquids Using X-Ray Reflectivity. *Mol. Phys.* **2001**, *99* (10), 795.
(30) Cremer, T.; Killian, M.; Gottfried, J. M.; Paape, N.; Wasserscheid, P.; Maier, F.; Steinrück, H. P. Physical Vapor Deposition of [Emim][Tf_2N]: A New Approach to the Modification of Surface Properties with Ultrathin Ionic Liquid Films. *ChemPhysChem* **2008**, *9* (15), 2185.
(31) Liu, Y.; Zhang, Y.; Wu, G.; Hu, J. Coexistence of Liquid and Solid Phases of Bmim-PF_6 Ionic Liquid on Mica Surfaces at Room Temperature. *J. Am. Chem. Soc.* **2006**, *128* (23), 7456.
(32) Bovio, S.; Podesta, A.; Lenardi, C.; Milani, P. Evidence of Extended Solidlike Layering in [Bmim][NTf_2] Ionic Liquid Thin Films at Room-Temperature. *J. Phys. Chem. B* **2009**, *113* (19), 6600.
(33) Sobota, M.; Nikiforidis, I.; Hieringer, W.; Paape, N.; Happel, M.; Steinrück, H.-P.; Görling, A.; Wasserscheid, P.; Laurin, M.; Libuda, J. Toward Ionic-Liquid-Based Model Catalysis: Growth, Orientation, Conformation, and Interaction Mechanism of the [Tf_2N]$^-$ Anion in [Bmim][Tf_2N] Thin Films on a Well-Ordered Alumina Surface. *Langmuir* **2010**, *26* (10), 7199.
(34) Maruyama, S.; Takeyama, Y.; Taniguchi, H.; Fukumoto, H.; Itoh, M.; Kumigashira, H.; Oshima, M.; Yamamoto, T.; Matsumoto, Y. Molecular Beam Deposition of Nanoscale Ionic Liquids in Ultrahigh Vacuum. *ACS Nano* **2010**, *4* (10), 5946.
(35) Biedron, A. B.; Garfunkel, E. L.; Castner, E. W., Jr; Rangan, S. Ionic Liquid Ultrathin Films at the Surface of Cu (100) and Au (111). *J. Chem. Phys.* **2017**, *146* (5), 054704.
(36) Xin, B.; Hao, J. Superhydrophobic Self-Assembled Monolayers of Long-Chain Fluorinated Imidazolium Ionic Liquids. *RSC Adv.* **2012**, *2*, 5141.
(37) Dhumal, N. R.; Noack, K.; Kiefer, J.; Kim, H. J. Molecular Structure and Interactions in the Ionic Liquid 1-Ethyl-3-Methylimidazolium Bis(Trifluoromethylsulfonyl)Imide. *J. Phys. Chem. A* **2014**, *118* (13), 2547.
(38) Hamm, P.; Zanni, M. T. *Concepts and Methods of 2D Infrared Spectroscopy*; Cambridge University Press: New York, 2011.
(39) Kraack, J. P.; Lotti, D.; Hamm, P. 2D Attenuated Total Reflectance Infrared Spectroscopy Reveals Ultrafast Vibrational Dynamics of Organic Monolayers at Metal-Liquid Interfaces. *J. Chem. Phys.* **2015**, *142* (21), 212413.
(40) King, J. T.; Kubarych, K. J. Site-Specific Coupling of Hydration Water and Protein Flexibility Studied in Solution with Ultrafast 2D-IR Spectroscopy. *J. Am. Chem. Soc.* **2012**, *134* (45), 18705.
(41) Roy, S.; Skoff, D.; Perroni, D. V.; Mondal, J.; Yethiraj, A.; Mahanthappa, M. K.; Zanni, M. T.; Skinner, J. L. Water Dynamics in Gyroid Phases of Self-Assembled Gemini Surfactants. *J. Am. Chem. Soc.* **2016**, *138* (8), 2472.

DOI: 10.1021/acscentsci.8b00353
ACS Cent. Sci. 2018, 4, 1065−1073

(42) Kwak, K.; Park, S.; Finkelstein, I. J.; Fayer, M. D. Frequency-Frequency Correlation Functions and Apodization in Two-Dimensional Infrared Vibrational Echo Spectroscopy: A New Approach. *J. Chem. Phys.* **2007**, *127* (12), 124503.
(43) Kwak, K.; Rosenfeld, D. E.; Fayer, M. D. Taking Apart the Two-Dimensional Infrared Vibrational Echo Spectra: More Information and Elimination of Distortions. *J. Chem. Phys.* **2008**, *128* (20), 204505.
(44) Kubo, R. A Stochastic Theory of Line Shapes. *Adv. Chem. Phys.* **2007**, *15*, 101.
(45) Del Pópolo, M. G.; Voth, G. A. On the Structure and Dynamics of Ionic Liquids. *J. Phys. Chem. B* **2004**, *108* (5), 1744.
(46) Sillescu, H. Heterogeneity at the Glass Transition: A Review. *J. Non-Cryst. Solids* **1999**, *243* (2−3), 81.
(47) Ediger, M. D. Spatially Heterogeneous Dynamics in Supercooled Liquids. *Annu. Rev. Phys. Chem.* **2000**, *51* (1), 99.
(48) Berthier, L.; Biroli, G.; Bouchaud, J.-P.; Cipelletti, L.; El Masri, D.; L'Hôte, D.; Ladieu, F.; Pierno, M. Direct Experimental Evidence of a Growing Length Scale Accompanying the Glass Transition. *Science* **2005**, *310* (5755), 1797.
(49) King, J. T.; Ross, M. R.; Kubarych, K. J. Ultrafast α-Like Relaxation of a Fragile Glass-Forming Liquid Measured Using Two-Dimensional Infrared Spectroscopy. *Phys. Rev. Lett.* **2012**, *108* (15), 157401.
(50) Hoffman, D. J.; Sokolowsky, K. P.; Fayer, M. D. Direct Observation of Dynamic Crossover in Fragile Molecular Glass Formers with 2D IR Vibrational Echo Spectroscopy. *J. Chem. Phys.* **2017**, *146* (12), 124505.
(51) Nugent, C. R.; Edmond, K. V.; Patel, H. N.; Weeks, E. R. Colloidal Glass Transition Observed in Confinement. *Phys. Rev. Lett.* **2007**, *99* (2), 025702.
(52) Richert, R. Dynamics of Nanoconfined Supercooled Liquids. *Annu. Rev. Phys. Chem.* **2011**, *62*, 65.

DOI: 10.1021/acscentsci.8b00353
ACS Cent. Sci. 2018, 4, 1065−1073